Supporting Information

Room Temperature Growth of $Co(OH)_2$ Nanosheets on Nanobelt-like $Cu(OH)_2$ Arrays For a Binder-free High Performance All-solid-state Supercapacitor

Biraj Kanta Satpathy,[a] Satyaroop Patnaik,[b] and Debabrata Pradhan[a,b,*]

[a]*School of Nanoscience and Technology, Indian Institute of Technology Kharagpur, Kharagpur 721 302, India*

[b]*Materials Science Centre, Indian Institute of Technology Kharagpur, Kharagpur 721 302, India*

*E-mail: deb@matsc.iitkgp.ac.in

Equations used for the calculation of specific capacitances

$$C_{a1} = \frac{\int I_1(V)dV}{2\Delta V \times v \times S} \quad (1)$$

$$C_{g1} = \frac{\int I_1(V)dV}{2\Delta V \times v \times m} \quad (2)$$

$$C_{a2} = \frac{I_2 \times \Delta t}{\Delta V \times S} \quad (3)$$

$$C_{g2} = \frac{I_2 \times \Delta t}{\Delta V \times m} \quad (4)$$

$$C_v = \frac{I_2 \times \Delta t}{\Delta V \times v} \quad (5)$$

where $\int I_1(V)dV$ represents the area enclosed by the CV curve, ΔV is the potential window and v is the scan rate. C_{a1} and C_{a2} (F cm^{-2}) are the areal capacitances measured from the CV and GCD curves, respectively. I_1(A) is the response current, I_2(A) is the applied current, Δt is the discharge time, and S (cm^2) is the geometrical area of the active electrode material, m is the mass of active material, and v is the volume of active material (including CF).

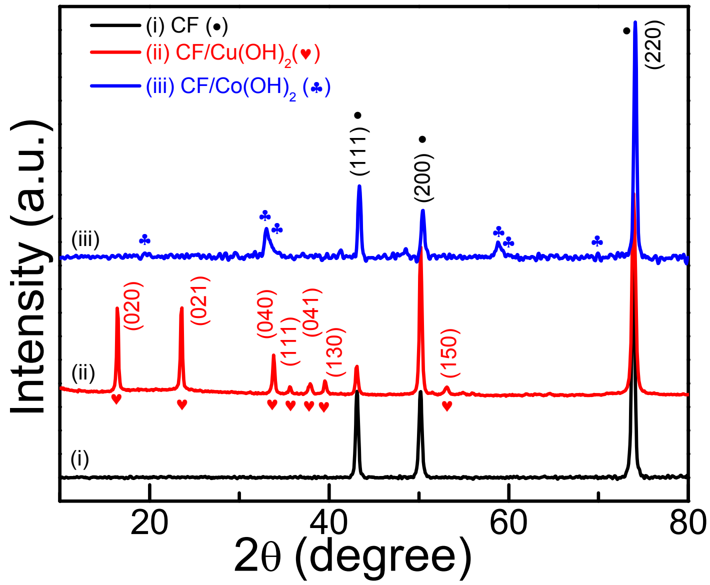

Figure S1. XRD patterns of (i) Cu foil (CF) matched with JCPDS file 04-009-2090, (ii) $Cu(OH)_2$ matched with JCPDS file 00-013-0420, and (iii) $Co(OH)_2$ matched with JCPDS file 00-002-0925.

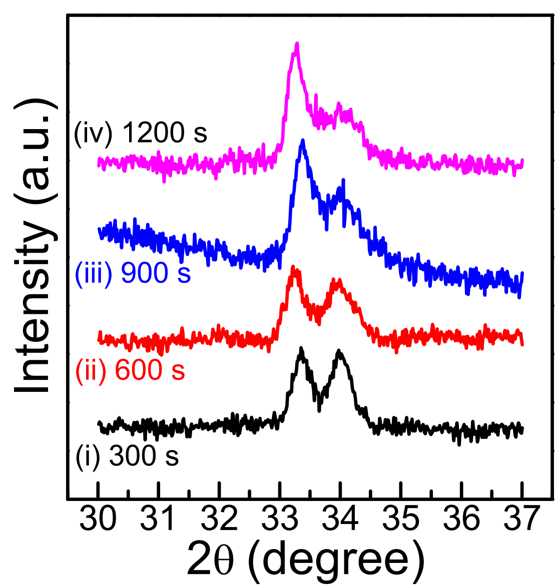

Figure S2. XRD patterns of $Co(OH)_2$ films electrodeposited for different durations, i.e. (i) 300 s, (ii) 600 s, (iii) 900 s, and (iv) 1200 s. The XRD patterns show the region of $Co(OH)_2$ diffraction peaks only.

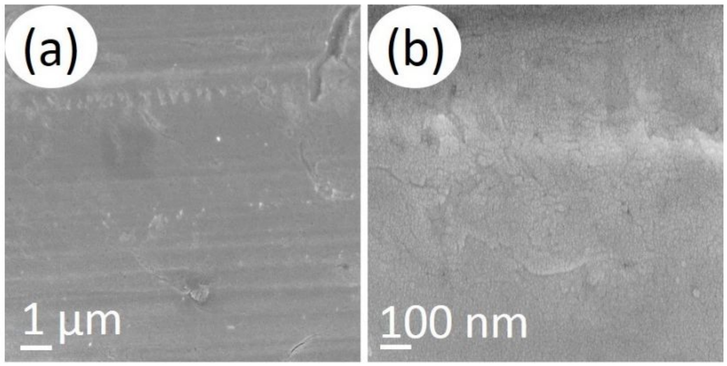

Figure S3. FESEM images of CF used as a substrate for the synthesis of $Cu(OH)_2$ and electrodeposition of $Co(OH)_2$. (a) low and (b) high magnification FESEM images of CF.

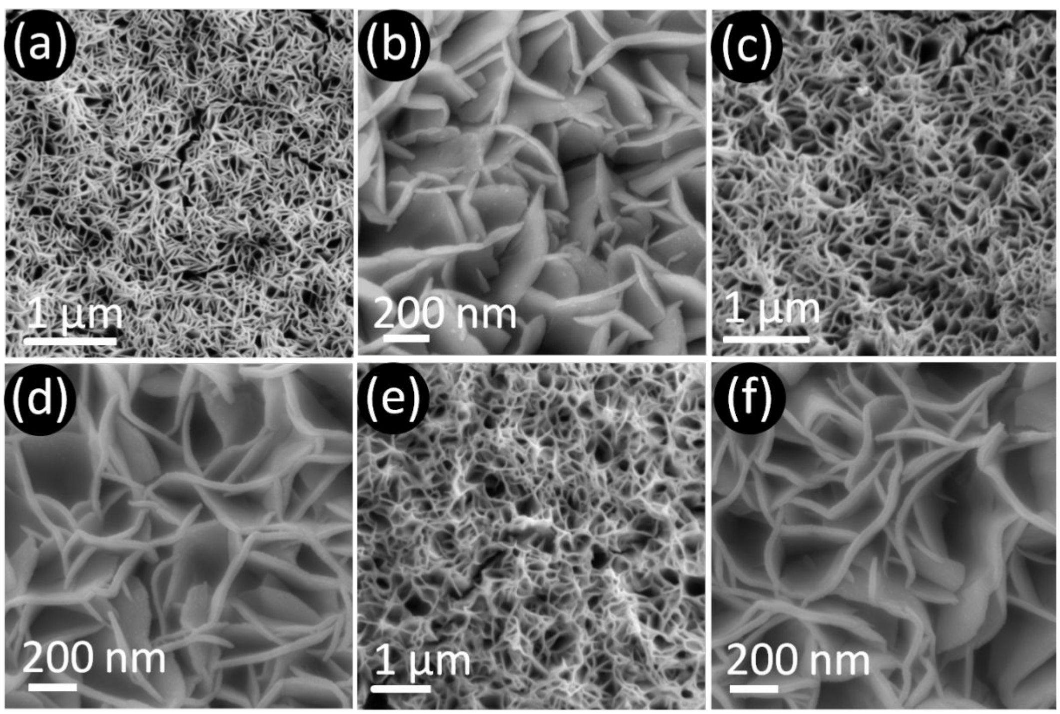

Figure S4. FESEM images of electrodeposited $Co(OH)_2$ on the CF for (a,b) 1200 s (c,d) 600 s and (e,f) 300 s.

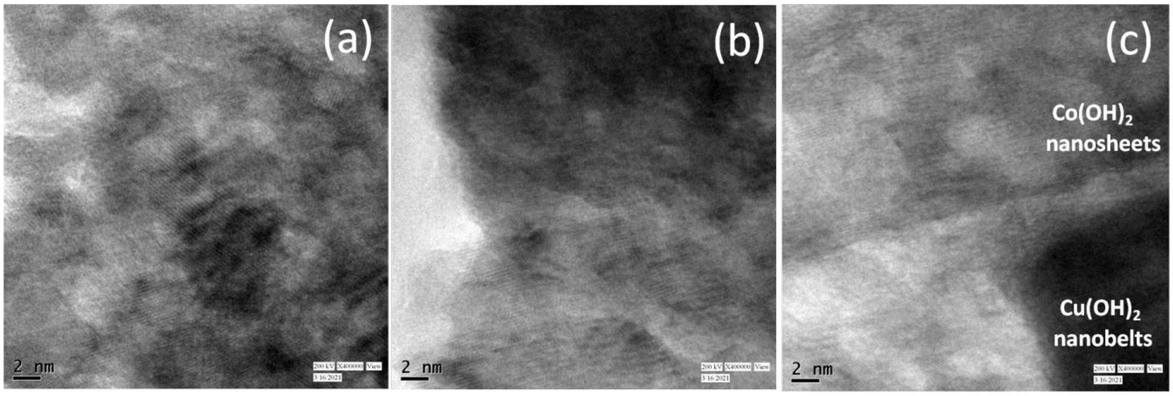

Figure S5. TEM images of $Cu(OH)_2/Co(OH)_2$. (a) $Cu(OH)_2$ nanobelt region, (b) $Co(OH)_2$ nanosheet region and (c) interface of $Cu(OH)_2$ and $Co(OH)_2$.

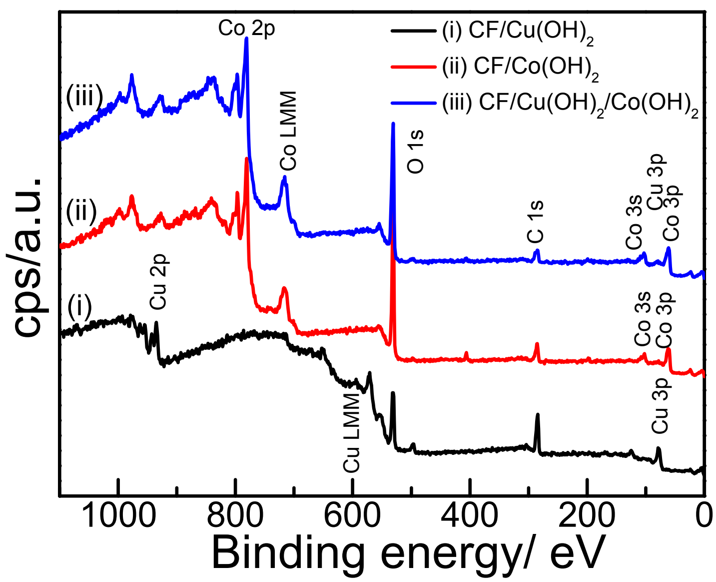

Figure S6. XPS survey spectra of (i) $CF/Cu(OH)_2$, (ii) $CF/Co(OH)_2$, and (iii) $CF/Cu(OH)_2/Co(OH)_2$.

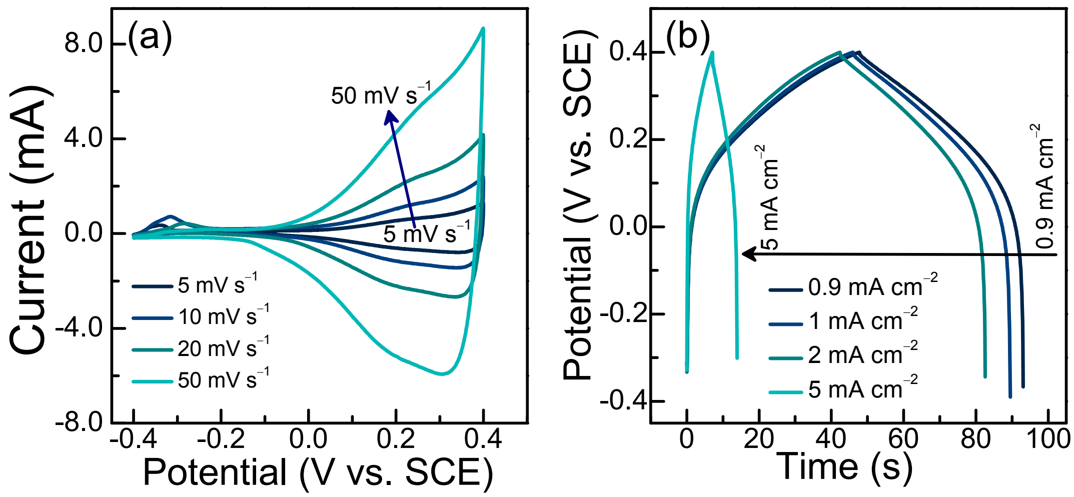

Figure S7. (a) Cyclic voltammetry and (b) galvanostatic charge discharge curves for $CF/Cu(OH)_2$ in 6 M KOH at different scan rates and current densities, respectively.

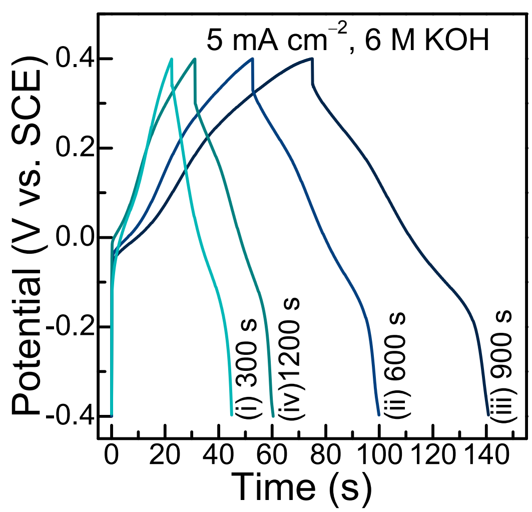

Figure S8. Galvanostatic charge discharge curves for the $Co(OH)_2$ layer electrodeposited for the duration of (i) 300 s, (ii) 600 s, (iii) 900 s, and (iv) 1200 s on $CF/Cu(OH)_2$ in 6 M KOH at 5 mA cm^{-2} current density, respectively.

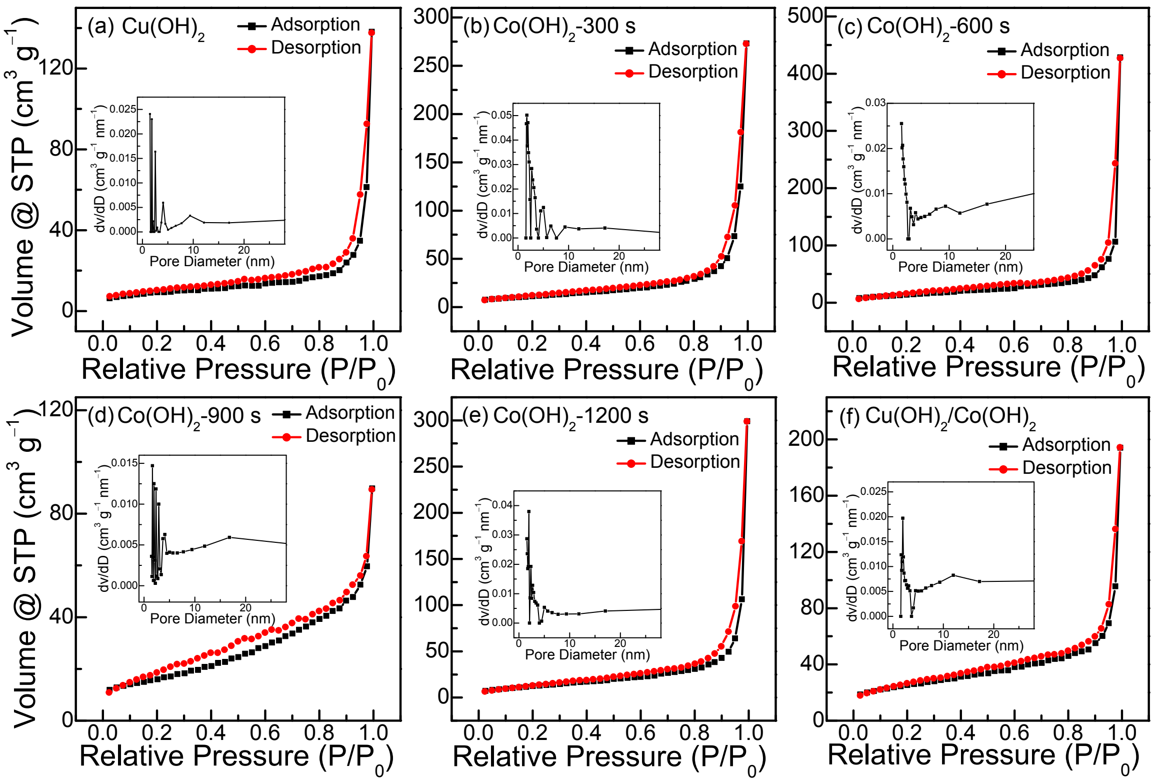

Figure S9. N_2 adsorption and desorption isotherms for (a) $Cu(OH)_2$ nanobelts, (b-e) $Co(OH)_2$ nanosheets (300, 600, 900 and 1200s), and (f) $Cu(OH)_2/Co(OH)_2$ hybrid material. Insets show the BJH pore size distribution.

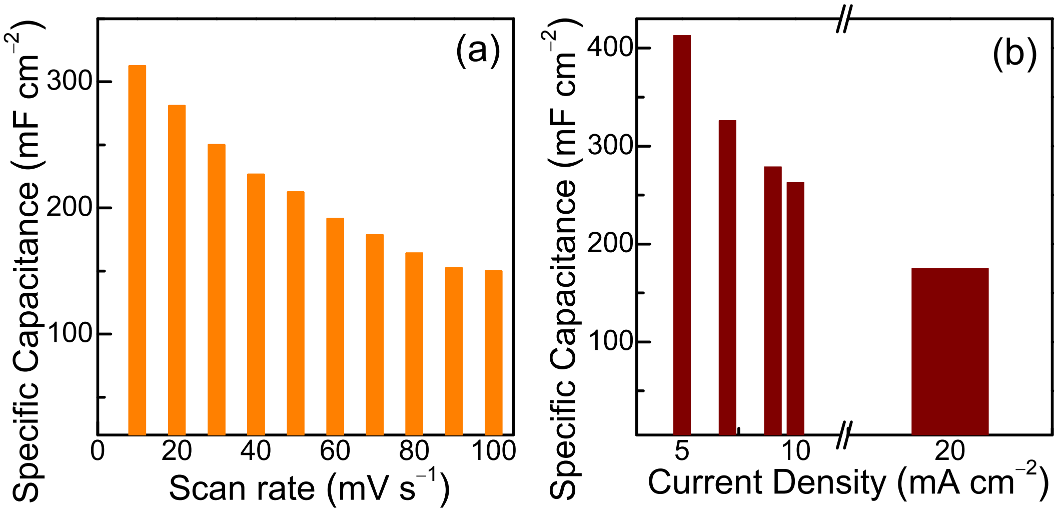

Figure S10. Areal specific capacitances as a function of (a) scan rate and (b) current density for $CF/Cu(OH)_2/Co(OH)_2$ in 6 M KOH.

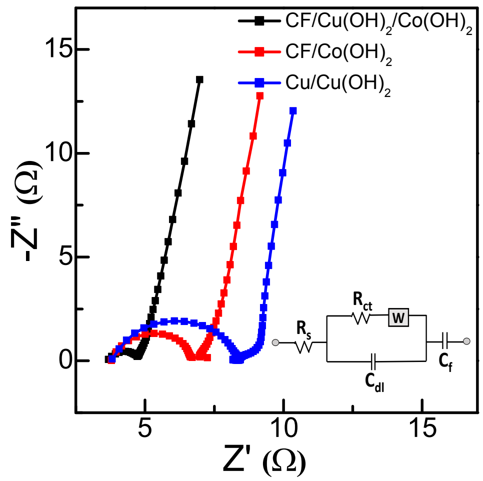

Figure S11. EIS spectra of the CF/Cu(OH)$_2$ and CF/Co(OH)$_2$ and CF/Co(OH)$_2$/Cu(OH)$_2$ of the frequency range of 0.01 Hz to 1 MHz in a three-electrode configuration in 6 M KOH electrolyte.

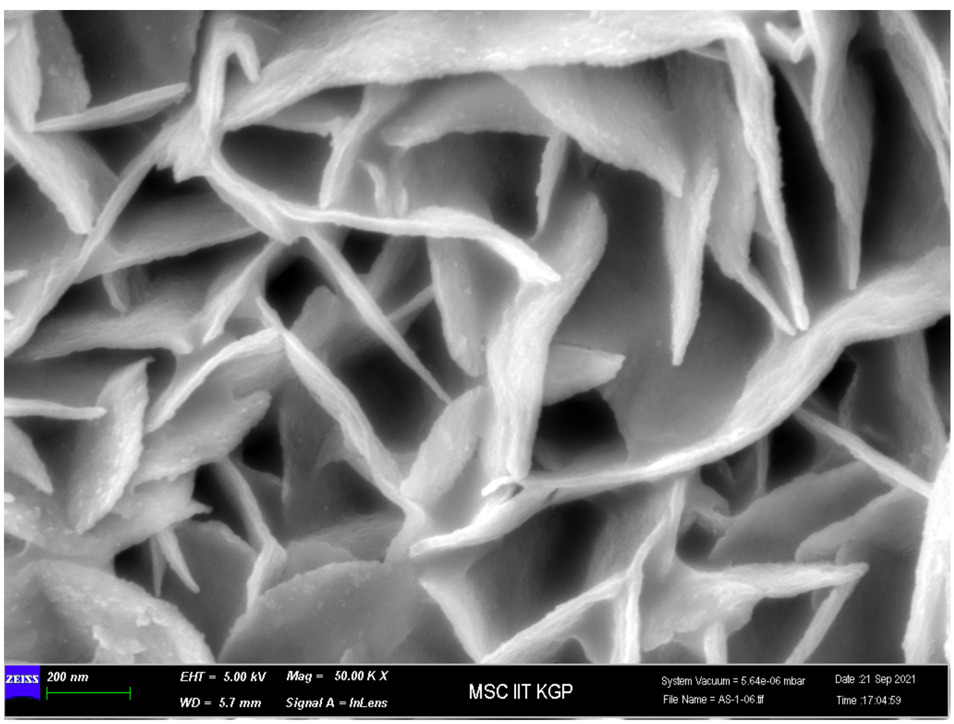

Figure S12. FESEM image of CF/Co(OH)$_2$/Cu(OH)$_2$ electrode after 12000 GCD cycles in 6 M KOH electrolyte.

Table S1. Comparison of various electrochemical parameters of supercapacitor device with similar other electrode materials synthesized by different methods, such as electrochemical deposition (ECD) and chemical vapour deposition (CVD).

Electrode materials	*Current collector*	*Synthesis method*	*Electrolyte*	*Voltage window*	*Capacitance*	*Energy Density*	*Stability*
CF/AC//Co(OH)$_2$/Cu(OH)$_2$/CF (This work)	Cu	ECD	PVA-KOH	0–1.5 V	113 mF cm^{-2}@2.5 mA cm^{-2}	3.5×10^{-2} mWh cm^{-2}@ 1.87 mW cm^{-2}	81.7% for 12000 cycles
Cu(OH)$_2$‖FeOOH[1]	Cu	Printing process	[EMIM][BF$_4$] ionic liquid	0–1.5 V	58 mF cm^{-2}@ 0.1 mA cm^{-2}	18.07 µWh cm^{-2}@~0.05 µW cm^{-2}	82% for 10000 cycles
Cu@Ni/porousNi/MnCo$_2$O$_4$ symmetric device[2]	Cu	ECD	PVA-KOH	0–1.3 V	21 mF cm^{-2}@ 1.8 mA cm^{-2}	12.8 µWh cm^{-2}@ 110 µW cm^{-2}	93.7% for 5000 cycles
CuO/3DGN/CC* symmetric device[3]	Carbon cloth	CVD	PVA-LiCl	0–0.8 V	64 mF cm^{-2}@ 0.25 mA cm^{-2}	5.9 µWh cm^{-2}@ 110 µW cm^{-2}	86% for 5000 cycles
Cu$_2$O/Cu/graphite complex‖CP[4]	Cellulose fibers	Pencil drawing and ECD	6 M KOH	0–0.8 V	122 mF cm^{-2}@ 1 mA cm^{-2}	10.8 µWh cm^{-2}@ 402.5 µW cm^{-2}	95.3% for 8000 cycles
RGO@CoNi-LDH‖RGO@AC[5]	RGO	ECD	PVA-KOH	0–1.2 V	178mF cm^{-2}@ 3.5 mA cm^{-2}	8.89 µWh cm^{-2}@ 0.525 mW cm^{-2}	95.3% for 2000 cycles
Co(OH)$_2$‖Co(OH)$_2$[6]	Cu	ECD	6 M KOH	0–1.0 V	1.29 mF cm^{-2}@ 0.5 mA cm^{-2}	0.46µWh cm^{-2}@ 422µW cm^{-2}	138% for 2000 cycles
Vanadium/CoO on carbon nanofibers[7]	Ni foam	Electrospinning	PVA-KOH	0–1.4 V	~155 mF cm^{-2}@ 4 mA cm^{-2}	44.2µWh cm^{-2}@ 2.8 mW cm^{-2}	95.2% for 10000 cycles
Co$_3$O$_4$ nanosheets on porous carbon (symmetric)[8]	Ni foam	Hydrothermal	PVA-KOH	0–1.4 V	130 mF cm^{-2}@ 0.5 mA cm^{-2}	40.5 µWh cm^{-2}@ 0.74 mW cm^{-2}	87.1% for 3000 cycles

Table S2. Comparison of volumetric energy density of ASC devices with different active hydroxide materials.

Electrode materials	*Volumetric Energy Density (mWh cm⁻³)*	*Volumetric Power Density (mW cm⁻³)*
$CF/AC//Co(OH)_2/Cu(OH)_2/CF$ (This work)	14.06	750
3D $Cu(OH)_2$[9]	4.152	383.2
$Cu(OH)_2$‖FeOOH[1]	10.03	-
NiCo-LDH‖Textile carbon[10]	7.4	103
NiCo-LDH‖NiCo-LDH[11]	1.25	47.4
Zn–Ni–Co TOH-130‖FEG[12]	2.43	6
$Ni(OH)_2$–$Co(OH)_2$/NiSe–Ni_3S_2/NF‖AC/NF[13]	13.9	200
MORGO/NiCo-LDH[14]	5.1	180
Cu_3N@CoFe-LDH/Cu‖AC/Ni[15]	2.47	15
Ni/Co-3500‖OCC[16]	4.35	60.1

References

[1] Xie, J.-Q.; Ji, Y.-Q.; Kang, J.-H.; Sheng, J.-L.; Mao, D.-S.; Fu, X.-Z.; Sun, R.; Wong, C.-P. In Situ Growth of $Cu(OH)_2$@FeOOH Nanotube Arrays on Catalytically Deposited Cu Current Collector Patterns for High-Performance Flexible in-Plane Micro-Sized Energy Storage Devices. *Energy Environ. Sci.* **2019**, *12* (1), 194–205. https://doi.org/10.1039/C8EE01979G.

[2] Ji, Y.; Xie, J.; Wu, J.; Yang, Y.; Fu, X.-Z.; Sun, R.; Wong, C.-P. Hierarchical Nanothorns $MnCo_2O_4$ Grown on Porous/Dense Ni Bi-Layers Coated Cu Wire Current Collectors for High Performance Flexible Solid-State FiberSupercapacitors. *J. Power Sources* **2018**, *393*, 54–61. https://doi.org/https://doi.org/10.1016/j.jpowsour.2018.04.109.

[3] Li, Y.; Wang, X.; Yang, Q.; Javed, M. S.; Liu, Q.; Xu, W.; Hu, C.; Wei, D. Ultra-Fine CuO Nanoparticles Embedded in Three-Dimensional Graphene Network Nano-Structure for High-Performance Flexible Supercapacitors. *Electrochim. Acta* **2017**, *234*, 63–70. https://doi.org/10.1016/j.electacta.2017.02.167.

[4] Wan, C.; Jiao, Y.; Li, J. Multilayer Core–Shell Structured Composite Paper Electrode Consisting of Copper, Cuprous Oxide and Graphite Assembled on Cellulose Fibers for Asymmetric Supercapacitors. *J. Power Sources* **2017**, *361*, 122–132. https://doi.org/10.1016/j.jpowsour.2017.06.070.

[5] Yin, Q.; Li, D.; Zhang, J.; Zhao, Y.; Wang, C.; Han, J. CoNi-Layered Double Hydroxide Array on Graphene-Based Fiber as a New Electrode Material for Microsupercapacitor. *Appl. Surf. Sci.* **2019**, *487*, 1–8. https://doi.org/10.1016/j.apsusc.2019.04.253.

[6] Kalasina, S.; Pattanasattayavong, P.; Suksomboon, M.; Phattharasupakun, N.; Wutthiprom, J.; Sawangphruk, M. A New Concept of Charging Supercapacitors Based on the Photovoltaic Effect. *Chem. Commun.* **2017**, *53* (4), 709–712. https://doi.org/10.1039/C6CC08131B.

[7] Nie, G.; Zhao, X.; Jiang, J.; Luan, Y.; Shi, J.; Liu, J.; Kou, Z.; Wang, J.; Long, Y.-Z. Flexible Supercapacitor of High Areal Performance with Vanadium/cobalt oxides on Carbon Nanofibers as a Binder-free Membrane Electrode. *Chem. Eng. J.* **2020**, *402*, 12694. https://doi.org/10.1016/j.cej.2020.126294.

[8] Ji, Y.; Deng, Y.; Chen, F.; Wang, Z.; Lin, Y.; Guan, Z. Ultrathin Co_3O_4 Nanosheets Anchored on Multi-heteroatom Doped Porous Carbon Derived from Biowaste for High Performance Solid-state Supercapacitors. *Carbon* **2020**, *156*, 359–369. https://doi.org/10.1016/j.carbon.2019.09.064.

[9] He, D.; Wang, G.; Liu, G.; Bai, J.; Suo, H.; Zhao, C. Facile Route to Achieve Mesoporous $Cu(OH)_2$Nanorods on Copper Foam for High-Performance Supercapacitor Electrode. *J. Alloys Compd.* **2017**, *699*, 706–712. https://doi.org/10.1016/j.jallcom.2016.12.398.

[10] Zhi, L.; Zhang, W.; Dang, L.; Sun, J.; Shi, F.; Xu, H.; Liu, Z.; Lei, Z. Holey Nickel-Cobalt Layered Double Hydroxide Thin Sheets with Ultrahigh Areal Capacitance. *J. Power Sources* **2018**, *387*, 108–116. https://doi.org/10.1016/j.jpowsour.2018.03.063.

[11]Jeong, Y. M.; Son, I.; Baek, S. H. Binder–Free of NiCo–Layered Double Hydroxides on Ni–Coated Textile for Wearable and Flexible Supercapacitors. *Appl. Surf. Sci.* **2019**, *467–468*, 963–967. https://doi.org/10.1016/J.APSUSC.2018.10.252.

[12] Huang, Z.-H.; Sun, F.-F.; Batmunkh, M.; Li, W.-H.; Li, H.; Sun, Y.; Zhao, Q.; Liu, X.; Ma, T.-Y. Zinc–Nickel–Cobalt Ternary Hydroxide Nanoarrays for High-Performance Supercapacitors. *J. Mater. Chem. A* **2019**, *7* (19), 11826–11835. https://doi.org/10.1039/C9TA01995B.

[13]Xu, J.; Han, F.; Fang, D.; Wang, X.; Tang, J.; Tang, W. Hierarchical Bimetallic Hydroxide/Chalcogenide Core–Sheath Microarrays for Freestanding Ultrahigh Rate Supercapacitors. *Nanoscale* **2019**, *12* (1), 72–78. https://doi.org/10.1039/C9NR08418E.

[14]Jia, D.; Jiang, D.; Zheng, Y.; Tan, H.; Cao, X.; Liu, F.; Yue, L.; Sun, Y.; Liu, J. Electrochemical Synthesis of NiCo Layered Double Hydroxide Nanosheets Decorated on Moderately Oxidized Graphene Films for Energy Storage. *Nanoscale* **2019**, *11* (6), 2812–2822. https://doi.org/10.1039/C8NR08869A.

[15]Zhou, X.; Li, X.; Chen, D.; Zhao, D.; Huang, X. Ultrathin CoFe-Layered Double Hydroxide NanosheetsEmbedded in High Conductance Cu_3N Nanowire Arrays with a 3D Core–Shell Architecture for Ultrahigh Capacitance Supercapacitors. *J. Mater. Chem. A* **2018**, *6* (47), 24603–24613. https://doi.org/10.1039/C8TA09442J.

[16]Pan, M.; Zeng, W.; Quan, H.; Cui, J.; Guo, Y.; Wang, Y.; Chen, D. Low-Crystalline Ni/Co-OxyhydroxidesNanoarrays on Carbon Cloth with High Mass Loading and Hierarchical Structure as Cathode for Supercapacitors. *Electrochim. Acta* **2020**, *357*, 136886. https://doi.org/10.1016/j.electacta.2020.136886.